

Strengthening in Gold Nanopillars with Nanoscale Twins

Konstantin A. Afanasyev[†] and Frederic Sansoz^{*‡}

*Physics Department, The University of Vermont, Burlington, Vermont 05405, and
School of Engineering, The University of Vermont, Burlington, Vermont 05405*

Received April 23, 2007; Revised Manuscript Received May 18, 2007

ABSTRACT

The role of growth twin boundaries on the slip activity of gold nanopillars under uniaxial compression was investigated by molecular dynamics simulation. A new type of size-dependent strengthening was found in twinned gold nanopillars. Strengthening resulted from slip arrests in the form of Lomer–Cottrell locks at the intersection of partial dislocations and twin boundaries. The significance of such phenomenon was found to depend on the twin size. These findings could help engineers design tunable mechanical properties in nanowires by interfacial plasticity.

Gold nanorods and nanowires play a central role in a wide variety of molecular applications from energy conversion¹ to biological sensing and gene delivery.² Considerable interest has been drawn into controllably synthesizing Au nanowires and understanding their size dependence on mechanical, electrical, photonic, and optical properties.^{3–6} Template-assisted electrodeposition into small pores is a technique commonly used to process Au nanowires and nanopillars on a large scale.^{7–14} The structure of electrodeposited Au nanowires has been investigated using transmission electron microscopy (TEM) and X-ray diffraction.^{11–12} TEM studies have revealed that 90% of Au nanowires fabricated by electrodeposition are fcc cylindrical crystals with [111] growth direction.¹¹ In this letter, we use molecular dynamics simulation to describe a new type of size-dependent strengthening governed by interfacial plasticity in $\langle 111 \rangle$ -oriented Au nanopillars consisting of growth twin boundaries.

Size scale effects on strength and plasticity in nanosized metals can be divided into geometry-dependent and microstructure-dependent effects. Geometric size effects on Au crystal plasticity have first been observed at the submicrometer scale by Greer and Nix^{3,15} using compression tests on micromachined and electroplated micro/nanopillars. These authors proposed that the overall sample dimensions artificially limit the length scale available for plastic processes and thereby significantly increase the material yield strength. A mechanism has been invoked to account for the size scale dependence based on dislocation starvation³ in which the density of mobile dislocations created from pre-existing sources is counterbalanced by the density of dislocations escaping the crystal. Atomistic simulations have also been

used to elucidate the nature of slip activity in $\langle 111 \rangle$ -oriented Au nanowires.^{16–22} These have revealed that the slip activity at the onset of single-crystal plasticity occurs via the nucleation and propagation of $\{111\}\langle 112 \rangle$ partial slip and microtwins. Diao et al.¹⁶ noted that, in small single-crystal Au nanowires, the effects of surface stresses can cause size-dependence and compression/tension asymmetry on yield strength. However, the change of magnitude in yield stress has been found to be limited for small $\langle 111 \rangle$ -grown Au nanowires. It is also clear that the surface structure of the nanowire plays a crucial role on the dislocation nucleation process.^{18,20} Size-dependent strengthening has been confirmed experimentally by Wu et al.²¹ in electrodeposited Au nanobeams as small as 40 nm in diameter, where a 100-fold increase in yield stress was found as compared to their bulk counterpart. These authors have also observed that the strength of Au nanowires decreases after annealing, which supports the idea that microstructure-related size effects also exist in electrodeposited Au nanowires.

The microstructure of $\langle 111 \rangle$ -oriented Au nanowires can be varied by controlling the density of coherent growth twin boundaries with the electrochemical environment during deposition.^{11,12} The predominant twinning system in Au nanowires is (111)[112]. This system forms planar stacking faults extending through the cross-section of the wire, perpendicularly to the long axis. Growth nanotwins are known to strongly influence the plastic behavior in bulk metals with low stacking energy such as pure Cu^{23–25} and austenitic stainless steels.^{26–27} In nanotwinned metals, a decrease of twin interspacing, i.e., the average distance that a dislocation needs to span when traveling from one twin boundary to another during plastic deformation, results in a dramatic increase in material strength and hardening at the nanoscale. However, such a microstructure-related size effect

* To whom correspondence should be addressed. E-mail: frederic.sansoz@uvm.edu. Telephone: 802 656 3837. Fax: 802 656 1929.

[†] Physics Department, The University of Vermont.

[‡] School of Engineering, The University of Vermont.

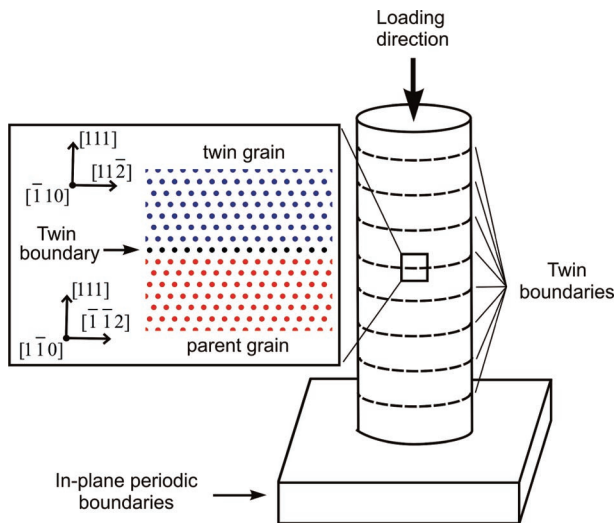


Figure 1. Schematic representation of a gold nanopillar with eight growth twins. Close up view on the atomic structure and orientation at twin boundaries.

has never been fully investigated in nanosized Au wires or pillars. A first attempt using atomistic simulation has been made by Hyde et al.¹⁸ to characterize the effect of one growth twin boundary located inside a $\langle 111 \rangle$ -oriented Au nanowire. These authors concluded that the twin itself was an effective obstacle against the propagation of dislocations but also did not appear to be source of dislocations. In twinned Cu nanowires, Wang and Huang²⁸ also discovered that the nature of the slip changes when partial dislocations are transmitted across twin boundaries, i.e., upon penetration, a dislocation with Burgers vector of $\frac{1}{2} \langle 110 \rangle$ can nucleate and glide on a $\{100\}$ plane instead of conventional $\{111\}$ planes. However, size effects on plasticity due to microstructure remained unknown in twinned Au nanowires.

Large-scale molecular dynamic simulations were conducted using an embedded atom method (EAM) potential for Au²⁹ identical to that used by Diao et al.¹⁶ and Hyde et al.¹⁸ The simulated geometry consisted of a cylindrical rod of 12.2 nm in diameter and 36 nm in height standing on a 3.5 nm thick Au film (Figure 1). The long axis of the pillar and normal to the film were both oriented along the $[111]$ direction. The model included 0.5 million atoms. Periodic boundaries were imposed on each side of the Au film in order to simulate the characteristic of a nanorod array. The simulations were performed in constant NVT ensemble with velocity-Verlet integrator and a time step of 0.005 ps. The model was first relaxed for 10 000 steps (50 ps) at 300 K and zero force. Compression was performed on the relaxed structure at the same temperature by displacing the top layer of atoms by increments of 0.55 Å, while fixing the bottom atom layer in the film. The pillar was then relaxed between each increment in displacement for 50 ps. The corresponding average strain rate was $2.7 \times 10^7 \text{ s}^{-1}$. Temperature was controlled using a Nosé–Hoover thermostat. The compression stress along the loading direction was calculated by adding the local atomic stress obtained from the Virial theorem over all the pillar atoms and dividing by the deformed pillar volume.³⁰ The resulting stress value was

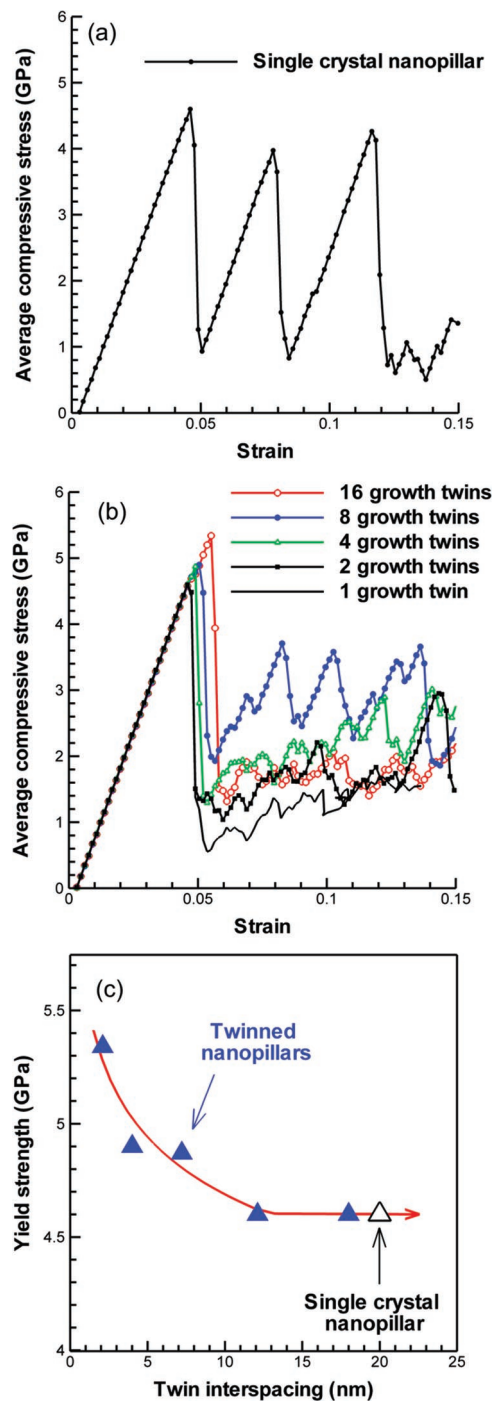


Figure 2. Uniaxial compression response of 12 nm diameter gold nanopillars with (a) single-crystal structure and (b) nanoscale twins. (c) Nanopillar strength as a function of twin interspacing.

averaged over 5000 steps (25 ps). We investigated one single-crystal structure and five twinned structures, as illustrated in Figure 1. The latter consisted of either 1, 2, 4, 8, or 16 twin boundaries, corresponding to a twin interspacing of 18.2, 12.2, 7.3, 4.1, and 2.1 nm, respectively.

Figure 2 represents the stress–strain response of all the pillars tested under uniaxial compression. We first present the case of a nanopillar with no twins (Figure 2a). The elastic modulus of the single-crystal nanopillar, which is determined using the first linear portion of the curve, is found equal to 114 GPa. This value is consistent with the Young’s modulus

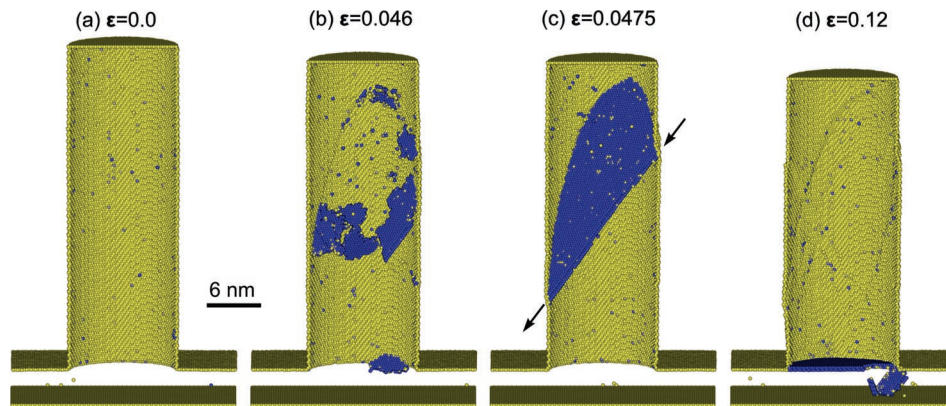


Figure 3. Cross-sectional view of a pristine gold nanopillar under uniaxial compression. (a) Initial pillar geometry before compression; (b) surface nucleation and propagation of a Shockley partial dislocation; (c) extended stacking fault and surface steps left after dislocation propagation; (d) evidence of dislocation escape after 12% compression. Atoms are colored based on their centrosymmetry. Atoms in gold color are surface atoms; atoms in blue color represent stacking faults. All other atoms are omitted. The compression strain (ϵ) is also shown.

for Au (116.2 GPa) reported in the literature.³⁰ The yield stress in the single-crystal case (4.58 GPa) is also in good agreement with the value on [111]-grown Au nanowires (4.8 GPa) obtained elsewhere by molecular dynamics.¹⁶ An important feature in the single-crystal response appears to be the significant serrated behavior marking the plasticity of the nanopillar. Particularly, such serration is characterized by a pronounced relaxation of stress (>3 GPa) at the elastic limit. The stress relaxation is followed by another linear regime during which the elastic strain builds up to a stress value approaching the yield strength. This process occurred three times in the single-crystal simulation, with additional stress peaks at 3.95 and 4.22 GPa for the second and third peaks, respectively.

Turning to the stress–strain response of Au nanopillars with nanoscale twins, Figure 2b shows that the plastic flow serration becomes significantly less pronounced in the presence of growth twins. Furthermore, strengthening is clearly apparent when the number of growth twins exceeds two, which corresponds to a twin interspacing less than or equal to the pillar diameter. More specifically, Figure 2c represents the evolution in nanopillar yield strength as a function of the twin interspacing. This figure shows that a clear correlation exists between twin size and strengthening in gold nanopillars for a twin interspacing smaller than 12 nm. For example, in the nanopillar consisting of eight growth twins, the related yield stress value is 4.83 GPa, which corresponds to a $\sim 6\%$ increase in strength over that of the single crystal. Note also in this case that the stress levels during plastic flow for strain above 5% are notably larger than in the other twinned pillar structures investigated.

To account for the different behaviors between single crystal and twinned nanopillars, we explore further the structure–property relationship by investigating the atomic mechanisms of plasticity. Our simulation results show three different stages of plastic deformation including the initial stage of dislocation emission and propagation, slip–boundary intersection, and interfacial plasticity. The first stage is found to proceed in the same manner for all pillar structures, i.e., by emission and glide of a perfect $(11\bar{1})[0\bar{1}\bar{1}]$ dislocation

emanating from the junction between pillar and film. It should be pointed out here that the strong stress gradient at the film–pillar junction seemed to play a dominant role on the dislocation emission process because the first dislocation nucleated glides on a slip system, which does not possess the highest Schmid factor (0.272). Furthermore, we find that the important stress decrease observed at the plasticity onset in Figure 2a,b is predominantly due to the second stage of deformation, which strongly varies between single crystal and twinned nanopillars.

We define the second stage of plasticity as the intersection of slip dislocations with the pillar microstructure including twin boundaries and free surfaces. In the single-crystal pillar, only intersections with free surfaces prevail. In this case, the second plasticity stage is dictated by the escape of dislocations at free surfaces when gliding from their nucleation site. Figure 3 illustrates this mechanism. Figure 3b shows the surface emission and propagation of a $(111)[121]$ Shockley partial dislocation at a compressive strain of 4.6%. The Schmid factor corresponding to this slip is high (0.314), which results in a significant decrease in stress as shown in Figure 2a. In Figure 3c, the partial dislocation has escaped the pillar at 4.75% strain, thereby forming an extended stacking fault and two surface steps. Following this event, a trailing partial dislocation is emitted on the same slip plane and glides on the $[\bar{1}12]$ slip direction. The propagation of this second partial causes perfect $[011]$ slip and leaves no dislocation debris inside the pillar.

This sequence appears to be closely related to the dislocation starvation model proposed in gold on sub-micrometer scale pillars.^{15,31} In our simulation, the dislocation-nucleation rate is equal to the dislocation-escape rate; therefore, no dislocation storage operates. At large compressive strain, other $\{111\}$ slip planes are also found to become active one by one. However, in the absence of strong obstacles to the propagation and escape of dislocations, the lattice structure of the pillar remains defect-free in the deformed state, similar to that of the pillar undergoing pure elastic loading. For example, it is worth noticing the absence of internal defects in the single-crystal pillar after 12%

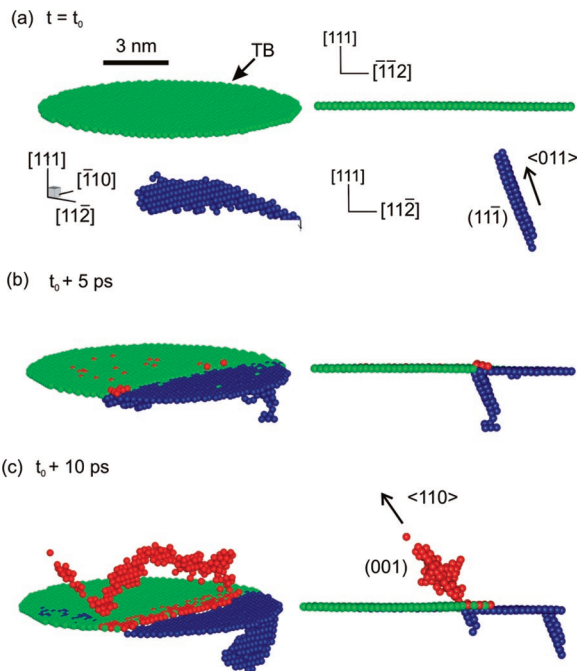
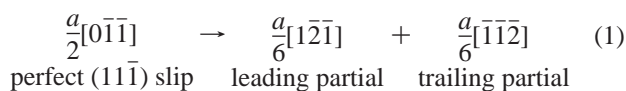


Figure 4. Intersection between slip dislocation and twin boundary (TB) in a twinned gold nanopillar. Atoms are colored based on their position with respect to the TB plane. Green-colored atoms are present in the initial TB plane. Blue-colored atoms below the TB plane represent the incident slip dislocation dissociated into two Shockley partials. Atoms in blue and red colors coinciding with the TB plane are atomic planes that have migrated along $[111]$ due to the propagation of interfacial dislocations. Red-colored atoms above the TB plane belong to the transmitted dislocation.

deformation (Figure 3d). This result therefore confirms the hypothesis that the mechanism of single-crystal plasticity is similar in nanosized and submicrometer scale pillars.

We now consider the second stage of plasticity in nanopillars consisting of twin boundaries, with a particular focus on those with a twin spacing smaller than or equal to the pillar diameter. In this type of structure, newly nucleated dislocations are not able to escape freely; the second stage is therefore related to dislocation-twin intersections. It is well-established that twin boundaries act as barriers for the propagation of dislocations.^{18,32–37} A typical twin-dislocation reaction is presented in Figure 4. Figure 4a shows a perfect slip dislocation emitted from the film–pillar junction as obtained in the dislocation nucleation stage. Such dislocation is dissociated into two Shockley partials gliding on the $(11\bar{1})$ slip plane and linked by a stacking fault. This type of reaction is known to be energetically favored in fcc metals with low stacking fault energy such as gold. Here, the dissociation reaction is given by:



Upon penetration of the leading partial into the twin boundary (Figure 4b), a portion of the twin interface is moved downward along the $[111]$ direction. Note that, in this

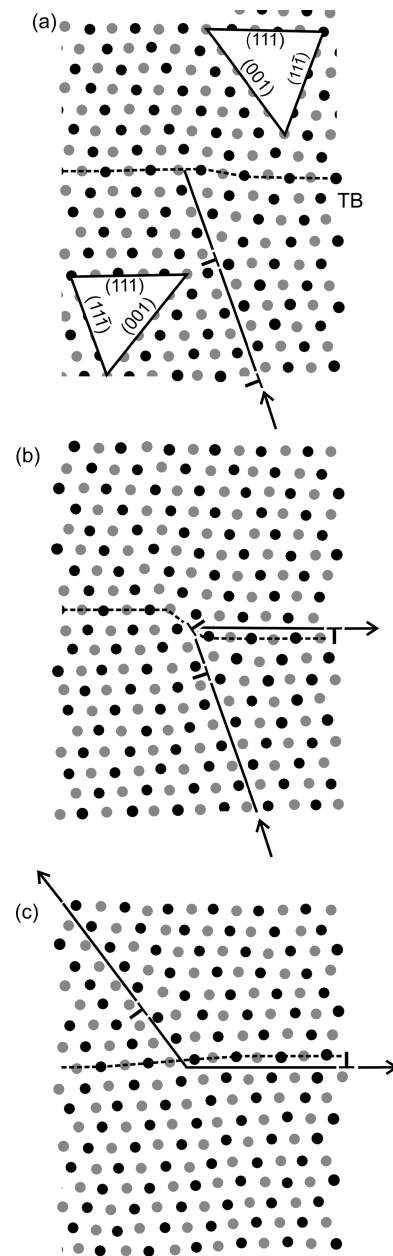


Figure 5. Atomic mechanism of interfacial plasticity at twin-slip intersection. Dark- and light-gray circles are atoms on different $\{110\}$ planes. Slip planes and twin boundaries are indicated by continuous and dashed lines, respectively. Slip directions are shown by arrows.

process, there is no dislocation transmitted from the parent grain to the twin grain. Furthermore, the stacking fault left behind the leading partial dislocation is stopped by the boundary. Figure 4c shows that the trailing partial, in turn, is absorbed into the twin boundary. The parent slip is then transmitted through the interface in the form of a $(001) \langle 110 \rangle$ dislocation in the twin grain. This type of reaction has also been observed by Wang and Huang²⁸ in Cu twinned nanowires subjected to uniaxial deformation. Slip on the (001) cut plane is not common in fcc metals. However, it is possible to observe (001) slip in gold when the cut plane is favorably oriented with respect to the loading axis, and the deformation involves the formation of Lomer–Cottrell

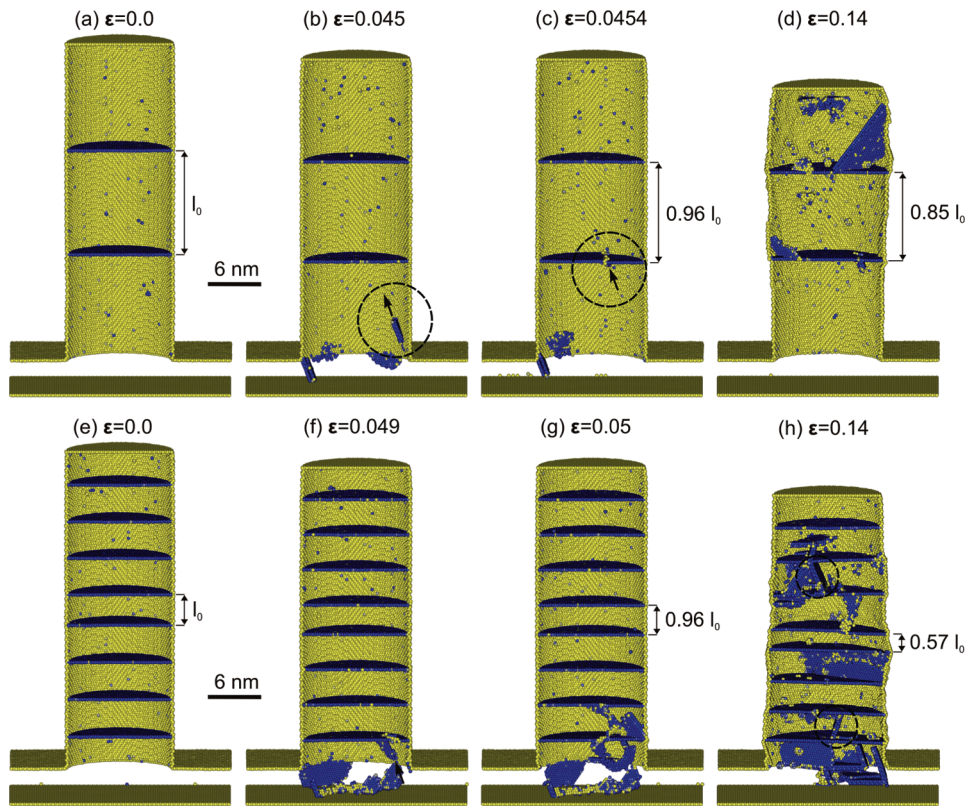


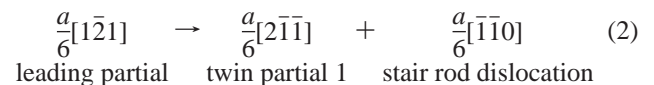
Figure 6. Cross-sectional view of twinned Au nanopillars under uniaxial compression. (a–d) Twin interspacing $l_0 = 12.2$ nm (two growth twins); (e–h) twin interspacing $l_0 = 4.1$ nm (eight growth twins).

locks.³² Both conditions are present in the example shown in Figure 4. The (001) cut plane has a Schmid factor (0.471) higher than that on any of the $\{111\}$ slip planes in the twin grain. Furthermore, it is shown hereafter that, upon twin-slip intersection, the product of glissile dislocations gliding on the twin boundary plane leads to the formation of Lomer–Cottrell locks, which are also known to contribute to strain hardening in bulk fcc metals.^{32,38}

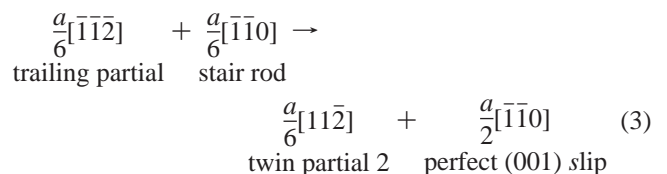
The transmission of screw dislocations across coherent twin boundaries has been studied in earlier works using molecular dynamics.^{35,37} Depending on the type of material, it was found that screw dislocations, which have a Burgers vector parallel to the twin plane, can either propagate into the adjacent twin grain by cutting through the boundary or be absorbed and dissociate within the boundary plane. These studies have clearly shown that the resistance to slip propagation across the interface, i.e., the strengthening effect, was strongly dependent on the nature of interfacial plasticity and underlying dislocation pathways. The source of strengthening due to interfacial plasticity also constitutes the third stage in the plastic deformation process of gold nanopillars.

Figure 5 presents the details of the dislocation dynamics at twin boundaries upon twin-slip intersection as obtained during our simulations. The dislocation reaction takes place in two parts. First, the leading partial dislocation in the incident slip is found to be absorbed by the interface. Dislocation dissociation occurs, which leaves a glissile displacement shift complete (DSC) partial dislocation on the twin plane and a sessile stair-rod dislocation pinned at the

twin-slip intersection. The corresponding reaction is given by



The combination of the stair-rod dislocation at the intersection of stacking faults on two $\{111\}$ slip planes contributes to form a Lomer–Cottrell lock (Figure 5b).³² It is worth mentioning that this configuration is very stable because the DSC twin dislocation can rapidly escape the pillar along the twin plane due to the small pillar diameter. It should also be noted that the migration of a portion of the twin boundary along $[111]$ can be interpreted from the glide of the DSC twin partial resulting from the lock formation (Figure 5b). Furthermore, when the trailing partial dislocation enters the twin plane as shown in Figure 5c, a second reaction takes place such as



Here, the trailing partial merges with the stair-rod dislocation obtained from the first reaction in order to form a new glissile DSC twin partial and a perfect $\langle 110 \rangle$ slip. The perfect $\langle 110 \rangle$ dislocation resulting from this reaction can only glide

along the symmetry plane of the lock, i.e., the (001) cut plane that is favorably oriented in the twin grain with respect to the loading direction. Also, the sign of the second DSC twin partial is opposite to that of the first DSC twin partial. As a result, the twin plane is found to move upward by one atom layer along the [111] direction; see Figure 5c. In this process, the initial twin boundary structure is recovered.

From an energetic perspective, the reaction in eq 2 is more favorable than that described by eq 3. This result implies that forming Lomer–Cottrell locks at the twin-slip intersection is made easier than transmitting the slip into a new (001) slip plane. In other words, the latter mechanism requires an increased driving force to occur. This factor plays a key role in the strengthening process of twinned nanopillars. Another strengthening factor can be attributed to the lack of slip transmission when steps are formed at twin boundaries after the formation of the Lomer–Cottrell locks. Such interruption of slip can be clearly seen in Figure 6 by comparing the effect of twin boundaries on the slip activity of gold nanopillars with either two or eight nanoscale twin boundaries (see corresponding movies in the Supporting Information). This figure shows a larger number of steps and stacking faults left at twin-slip intersections when the pillar consists of a small twin interspacing (eight growth twins in this case). It is also possible to observe significant changes in twin interspacing due to multiple steps formation when slip transmissions are not completely achieved. More specifically, Figure 6b shows that, at 14% compression, the variation in twin interspacing in the presence of two growth twins (~15%) can be directly correlated to the lattice deformation produced by the applied strain. In contrast, for the pillar consisting of eight twins, Figure 6h shows that the variation in twin interspacing is more significant (~43%) for the same level of applied strain, which would suggest that a large number of Lomer–Cottrell locks did not result in slip transmission.

Such phenomenon could be attributed to the fact that when the twin interspacing is of the same size than the splitting distance for dislocation dissociation, the trailing partial dislocation does not nucleate and the reaction in eq 3 cannot occur. This hypothesis is supported by the appearance of a large number of stacking faults joining two twin boundaries (see dashed circles in Figure 6h) in the pillar containing eight growth twins. This result is also confirmed on the nanopillar consisting of 16 twin boundaries (see corresponding movie in the Supporting Information). In the latter, it can be noted that the excess of stacking faults created at the plasticity onset is so large that an extended shear band is formed in the nanopillar. Also, this shear localization process can account for the difference in stress after post-yielding between nanopillars with eight and 16 twin boundaries (Figure 2b). In contrast, limited amount of residual stacking faults is found in the pillar with large twin interspacing (two growth twins) at 14% strain (Figure 6d).

In summary, we have found using molecular dynamics simulation that lattice dislocations can escape at free surfaces in single-crystal gold nanopillars under compression due to the absence of strong obstacle to their propagation. Such

mechanism is associated with a distinctive plasticity behavior that involves significant flow serration. This behavior leaves the pillar mostly defect-free even at large deformation. In contrast, the presence of growth twins, which can be introduced via current electrochemical methods, decreases the flow serration effect and tends to promote strengthening. This phenomenon has been related to slip arrests in the form of Lomer–Cottrell locks at the intersection between slip dislocation and twin boundary. We have also shown the dislocation reactions leading to the slip transmission at twin boundaries, by which glissile interfacial dislocations are created and propagate on the twin plane. The atomic mechanisms related to interfacial plasticity in gold nanopillars have also been found to depend on the twin size. The conclusions of our study provide a new approach to obtain size-dependent strengthening in nanowires by microstructure using interfacial plasticity.

Acknowledgment. Support from the Vermont Advanced Computing Center under Phase II NASA grant no. NNG 06GE87G is gratefully acknowledged. Atomistic simulations shown in this study have been performed using LAMMPS molecular dynamics simulator.³⁹

Supporting Information Available: Nanopillars consisting of 0, 2, 8, or 16 twin boundaries (AVI). This material is available free of charge via the Internet at <http://pubs.acs.org>.

References

- (1) Chou, C. H.; Chen, C. D.; Wang, C. R. *C. J. Phys. Chem. B* **2003**, *109*, 11135.
- (2) Bauer, L. A.; Birenbaum, N. S.; Meyer, G. J. *J. Mater. Chem.* **2004**, *14*, 517.
- (3) Greer, J.; Oliver, W. C.; Nix, W. D. *Acta Mater.* **2005**, *53*, 1821.
- (4) Rodrigues, V.; Ugarte, D. *Nanotechnology* **2002**, *13*, 404.
- (5) Barrelet, C. J.; Greytak, A. B.; Lieber, C., M. *Nano Lett.* **2004**, *4*, 1981.
- (6) Yu, Y.-Y.; Chang, S.-S.; Lee, C.-L.; Wang, C. R. *J. Phys. Chem. B* **1997**, *101*, 6661.
- (7) Forrer, P.; Schlottig, F.; Siegenthaler, H.; Textor, M. *J. Appl. Electrochem.* **2000**, *30*, 533.
- (8) Zhang, X. Y.; Zhang, L. D.; Lei, Y.; Zhao, L. X.; Mao, Y. Q. *J. Mater. Chem.* **2001**, *11*, 1732.
- (9) Wang, Z.; Su, Y.-K.; Li, H.-L. *Appl. Phys. A* **2002**, *74*, 563.
- (10) Walter, E. C.; Zach, M. P.; Favier, F.; Murray, B. J.; Inazu, K.; Hemminger, J. C.; Penner, R. M. *ChemPhysChem* **2003**, *4*, 131.
- (11) Tian, M.; Wang, J.; Kurtz, J.; Mallouk, T. E.; Chan, M. H. W. *Nano Lett.* **2003**, *3*, 919.
- (12) Wang, J.; Tian, M.; Mallouk, T. E.; Chan, M. H. W. *J. Phys. Chem. B* **2004**, *108*, 841.
- (13) Wang, X.-Y.; Zhong, H.; Yuan, J.-H.; Sheng, D.; Ma, X.; Xu, J.-J.; Chen, H.-Y. *Chem. Lett.* **2004**, *33*, 982.
- (14) Xu, C.; Zhang, L.; Zhang, H.; Li, H. *Appl. Surf. Sci.* **2005**, *252*, 1182.
- (15) Greer, J. R.; Nix, W. D. *Phys. Rev. B* **2006**, *73*, 245410.
- (16) Diao, J.; Gall, K.; Dunn, M. L. *Nano Lett.* **2004**, *4*, 1863.
- (17) Lin, J.-S.; Ju, S.-P.; Lee, W.-J. *Phys. Rev. B* **2005**, *72*, 085448.
- (18) Hyde, B.; Espinosa, H. D.; Farkas, D. *JOM* **2005**, September, 62.
- (19) Diao, J.; Gall, K.; Dunn, M. L.; Zimmerman, J. A. *Acta Mater.* **2006**, *54*, 643.
- (20) Rabkin, E.; Srolovitz, D. J. *Nano Lett.* **2007**, *7*, 101.
- (21) Rabkin, E.; Nam, H.-S.; Srolovitz, D. J. *Acta Mater.* **2007**, *55*, 2085.
- (22) Wu, B.; Heidelberg, A.; Boland, J. J. *Nat. Mater.* **2005**, *4*, 525.
- (23) Lu, L.; Shen, Y.; Chen, X.; Qian, L.; Lu, K. *Science* **2004**, *304*, 422.
- (24) Zhang, X.; Wang, H.; Chen, X. H.; Lu, L.; Lu, K.; Hoagland, R. G.; Misra, A. *Appl. Phys. Lett.* **2006**, *88*, 173116.
- (25) Dao, M.; Lu, L.; Shen, Y. F.; Suresh, S. *Acta Mater.* **2006**, *54*, 5421.
- (26) Zhang, X.; Misra, A.; Wang, H.; Nastasi, M.; Embury, J. D.; Mitchell, T. E.; Hoagland, R. G. *Appl. Phys. Lett.* **2004**, *84*, 1096.
- (27) Zhang, X.; Misra, A.; Wang, H.; Lima, A. L.; Hundley, M. F.; Hoagland, R. G. *J. Appl. Phys.* **2005**, *97*, 094302.

- (28) Wang, J.; Huang, H. *Appl. Phys. Lett.* **2006**, *88*, 203112.
- (29) Foiles, S. M.; Baskes, M. I.; Daw, M. S. *Phys. Rev. B* **1986**, *33*, 7983.
- (30) Diao, J.; Gall, K.; Dunn, M. L. *J. Mech. Phys. Solids* **2004**, *52*, 1935.
- (31) Tang, H.; Schwarz, K. W.; Espinosa, H. D. *Acta Mater.* **2006**, *55*, 1607.
- (32) Hirth, J. P.; Lothe, J., *Theory of Dislocations*; McGraw-Hill: New York, 1968.
- (33) Yamakov, V.; Wolf, D.; Phillpot, S. R.; Gleiter, H. *Acta Mater.* **2003**, *51*, 4135.
- (34) Couzinie, J. P.; Decamps, B.; Priester, L. *Int. J. Plast.* **2005**, *21*, 759.
- (35) Jin, Z.-H.; Gumbsch, P.; Ma, E.; Albe, K.; Lu, K.; Hahn, H.; Gleiter, H. *Scr. Mater.* **2006**, *54*, 1163.
- (36) Cao, A.; Wei, Y. *Phys. Rev. B: Condens. Matter Mater. Phys.* **2006**, *74*, 214108.
- (37) Zhu, T.; Li, J.; Samanta, A.; Kim, H. G.; Suresh, S. *Proc. Natl. Acad. Sci. U.S.A.* **2007**, *104*, 3031.
- (38) Baskes, M. I.; Hoagland, R. G.; Tsuji, T. *Modell. Simul. Mater. Sci. Eng.* **1998**, *6*, 9.
- (39) Plimpton, S. J. *J. Comp. Phys.* **1995**, *117*, 1, available at <http://lammmps.sandia.gov/>.

NL070959L